

# OPTICAL PHASE-LOCKED LOOP (OPLL) FOR AN AMPLITUDE MODULATED COMMUNICATIONS LINK USING SOLID STATE LASERS

Moe Z. Win, and Chien-Chung Chen

Jet Propulsion Laboratory, California Institute of Technology

4800 Oak Grove Drive, Pasadena, California, USA

Robert A. Scholtz

Communications Sciences Institute

RF-Systems 1 Department, University of Southern California

Los Angeles, California, USA

## ABSTRACT

Theoretical analysis is formulated for a solid state laser based optical phase-locked loop (OPLL) disturbed by shot noise, amplitude modulated noise, and frequency noise. The frequency noise spectral density of solid state lasers is modelled to contain a white component, a  $1/f$  component, and a strong  $1/f^2$  component at the laser output. This model is verified and spectral content of each component is measured using an open-loop RF frequency discriminator. The choice of loop filter is made by considering the frequency noise components, transient effects, and the loop damping factor  $\zeta$ . The total phase error variance as a function of loop bandwidth is displayed for several values of carrier signal-to-noise ratio for the measured frequency noise spectrum. Optimal loop bandwidth is also calculated as a function of carrier signal-to-noise ratio. An OPLL experiment is performed, and measured phase error variance is compared with the theoretical predictions using the measured frequency noise spectrum. The results show that the measured phase error variance closely matches the theoretical predictions.

## 1. INTRODUCTION

Coherent heterodyne optical communication technology can provide improved receiver sensitivity and better rejection capability of background noise over direct detection systems [1-2]. Coherent optical systems can benefit spacecraft navigation, call support potential space-based scientific experiments such as gravitational wave detection, and have strong potential for multiple-access communications over a single lasing bandwidth. In order to achieve the full advantage of heterodyne reception, it is desirable that an optical signal be coherently demodulated. Coherent demodulation is generally accomplished by synchronizing the incoming carrier with a local reference using a phase-locked loop (PLL) [3-4].

The performance of an OPLL operating with semiconductor lasers has been analyzed extensively by several authors. In most cases, the analyses were performed for a semiconductor laser based system supporting high data rate communications. For high data rate fiber optic links using semiconductor lasers, it is shown that the OPLL performance is dictated by the receiver shot noise and the white frequency noise. The performance of both heterodyne receiver and homodyne receiver has been analyzed by modeling the laser frequency noise as a white Gaussian noise process [4-5]. The treatment of the OPLL has also been extended to include  $1/f$  frequency noise [6-7].

However coherent phase tracking loops for diode-laser based systems require several megahertz of bandwidth because of the large linewidth of diode lasers [8], and the low signal power expected from some free-space links precludes the use of high bandwidth phase tracking loops. Consequently, development of free space communication systems employing semiconductor lasers have been confined to noncoherent heterodyne or direct detection systems. Recently, with the advances in diode-pumped solid state laser technology, sub-

KHz linewidth frequency stabilized lasers have been developed [9-14]. The high spectral purity of the frequency stabilized solid state laser is very desirable in applications such as free-space optical communications, where synchronization and retrieving of the received signal phase in the presence of weak incident signal power is required.

Initial application of the OPLL theory developed for semiconductor lasers [4, 5] to systems employing the frequency stabilized solid state lasers from Lightwave Electronics Inc., demonstrated that the measured phase error variance cannot be adequately explained by assuming that the frequency noise is dominated by the white frequency component [15-17]. In particular, the assumption that the laser frequency noise is dominated by white frequency noise has led to a predicted phase error variance that is 3-4 orders of magnitude larger than values that were experimentally measured using Lightwave lasers [16]. Furthermore, for a free space system, one would like to analyze the amplitude modulated channel. The amplitude modulated signal can be detected using either coherent (heterodyne) or noncoherent (direct) detection receivers and therefore permits a greater flexibility when interaction with a variety of receiver installations may be necessary.

In this paper, the design, analysis, and experimental verification of an OPLL based on Lightwave model 120-01A frequency-stabilized diode-pumped solid state lasers will be addressed. Specifically, the work will focus on the development of a new laser frequency noise model and its application to the design of an OPLL, operating under weak incident signal power.

## II. OPLL DESCRIPTION AND PERFORMANCE SUMMARY

Phase-locked loops have been analyzed extensively for communications systems using radio frequency (RF) [18, 19]. The stochastic integro-differential equation describing a

linearized OPLL can be derived, using similar approach as in RF systems, as

$$\frac{d\phi_e(t)}{dt} = f_N(t) - K_P \int_{-\infty}^{+\infty} [A\phi_e(\tau) + m(\tau) + n(\tau)] f_P(t - \tau) d\tau \quad (1)$$

where  $\phi_e(t)$  is the phase error,  $f_N(t)$  is the frequency noise process due to both the received signal and local oscillator (LO) laser,  $A^*$  is the average RF signal power,  $K_P$  is the tuning constant of the LO laser,  $n(t)$  is the additive noise, and  $f_P(t)$  denotes the impulse response of the tracking loop filter. The term  $m(t) = a(t) \sin[\phi_e(t)]$  is the modulation noise, due to amplitude modulation  $a(t)$ . In order to keep the analysis general, description of the modulation format will not be specified until section IV. The equivalent block diagram of the linearized OPLL describing (1) is shown in Fig. 1, where  $\phi_c(t)$  is the phase of the LO laser.

The closed loop transfer function is defined in the literature [18] as,

$$H_1(s) = \frac{AK_P F_P(s)}{s + AK_P F_P(s)}, \quad (2)$$

where  $F_P(s)$  is the loop filter transfer function (the Laplace transform of the impulse response of the loop filter). The transfer function from  $f_N(t)$  to  $\phi_e(t)$ ,  $H_2(s)$ , is related to the closed loop transfer function by

$$H_2(s) = [1 - H_1(s)] \frac{1}{s}. \quad (3)$$

The performance of the OPLL depends on the properties of the input signal and loop design. The performance is affected by shot noise, modulation noise, and frequency noise. When the loop is operating in the linear region, the effects of each noise can be determined separately and combined to obtain the net results [19]. Therefore, the total phase error variance can be written as

$$\sigma_{\phi_e}^2 = \sigma_{\phi_n}^2 + \sigma_{\phi_m}^2 + \sigma_{\phi_f}^2. \quad (4)$$

where  $\sigma_{\phi_n}^2$ ,  $\sigma_{\phi_m}^2$ ,  $\sigma_{\phi_f}^2$  are phase error variances due to additive noise, modulation noise, and frequency noise respectively.

The additive noise  $n(t)$ , due primarily to the LO shot noise, can be modelled as an additive white Gaussian noise with power spectral density (PSD)  $N_0$ . The phase error variance contributed by shot noise can be written as [19]

$$\sigma_{\phi_n}^2 = \frac{N_0}{42} B_L, \quad (5)$$

where  $B_L$  is the one sided loop bandwidth defined by

$$B_L = \int_0^{\infty} |H_1(j2\pi f)|^2 df. \quad (6)$$

For an amplitude modulated system, the modulation noise can be regarded as an amplitude noise, and can be treated in a similar fashion as the additive noise  $n(t)$  [15]. The PSD of the modulation noise  $m(t)$  is, in general, quite difficult to obtain because of the sinusoidal nonlinearity. However, it can be written using the linear approximation as  $m(t) = a(t)\phi_e(t)$ , when the phase error is small. Furthermore,  $a(t)$  and  $\phi_e(t)$  are assumed to be independent. This is a good approximation when the bandwidth of the loop filter is narrow compared to the data rate and hence  $\phi_e(t)$  is a function of a long history of  $a(t)$  which is composed of many independent data bits. By letting  $S_a(f)$  and  $S_{\phi_e}(f)$  be the PSD's of  $a(t)$  and  $\phi_e(t)$  processes respectively, the PSD of the amplitude modulated noise  $m(t)$  can be written as

$$S_m(f) = \int_{-\infty}^{+\infty} S_a(f - f') S_{\phi_e}(f') df'. \quad (7)$$

Typically,  $S_{\phi_e}(f)$  is very narrow compared to  $S_a(f)$ , and (7) can be approximated as

$$S_m(f) \approx \int_{-\infty}^{+\infty} S_a(f - f') \sigma_{\phi_e}^2 \delta_D(f') df' = \sigma_{\phi_e}^2 S_a(f) \quad (8)$$

where  $\sigma_{\phi_e}^2$  is the total phase error variance and  $\delta_D(f)$  is the Dirac-delta function. Therefore, the phase error variance due to modulation noise becomes

$$\sigma_{\phi_m}^2 = \sigma_{\phi_e}^2 \int_0^{\infty} |H_1(j2\pi f)|^2 S_a(f) df. \quad (9)$$

The phase error variance contributed by the frequency noise can be written as

$$\sigma_{\phi_f}^2 = \int_0^{\infty} |H_2(j2\pi f)|^2 S_f(f) df, \quad (10)$$

where  $S_f(f)$  is the PSD of frequency noise. As will be shown in the next section, the frequency noise of Lightwave model 120-01A lasers consists of three major components: a  $1/f$  or  $1/f^2$  component at low frequencies, a white frequency noise, and spectral peaks that correspond to relaxation oscillations. Mathematically the PSD of frequency noise is modelled as:

$$S_f(f) = k_0 + \frac{k_1}{f} + \frac{k_2}{f^2} \quad 0 < f < \infty, \quad (11)$$

By using the frequency noise model given by (11), the phase error variance contributed by the frequency noise can be written as

$$\sigma_{\phi_f}^2 = \int_0^{\infty} |H_2(j2\pi f)|^2 \left[ k_0 + \frac{k_1}{f} + \frac{k_2}{f^2} \right] df. \quad (12)$$

It can be shown that  $H_2(j2\pi f)$  has a ‘zero’ at  $f = 0$  for a perfect second-order loop, whereas first-order and imperfect second-order loops do not have this property. This property is very desirable since the ‘zero’ of  $H_2(j2\pi f)$  at  $f = 0$  will cancel the ‘poles’ of the  $1/f$  and  $1/f^2$  frequency noise components. Consequently, a perfect second-order loop can track out low frequency fluctuation that would occur when first-order or imperfect second-order loops are utilized. In terms of Doppler tracking, first-order and imperfect second-order loops can track the initial phase offset with zero steady state error but will result in a finite steady state error when tracking the frequency offset [18, 19]. A perfect

second-order loop has an advantage over first-order and imperfect second-order loops in that the former loop not only can track the phase and frequency offset with zero steady state error, but also can track the Doppler rate with finite steady state error [18, 19]. In terms of frequency acquisition, a perfect linearized second-order loop theoretically has an infinite pull-in range whereas first-order and imperfect second-order loops have finite pull-in ranges [18]. Furthermore, it is well known that perfect second-order loops are unconditionally stable [18, 19]. Hence a perfect second-order loop was chosen with the loop filter transfer function

$$L(s) = \frac{1 + \tau_2 s}{\tau_1 s^2}, \quad (13)$$

Using (2), (3), and section 2.161 of [20], along with algebraic simplifications, the phase error variance contributed by the frequency noise for a perfect second-order loop can be derived as

$$\sigma_{\phi}^2 = k_0 g_0(\zeta) \frac{1}{B_I} + k_1 g_1(\zeta) \frac{1}{B_I^2} + k_2 g_2(\zeta) \frac{1}{B_I^3} \quad (14)$$

where  $g_0(\zeta)$ ,  $g_1(\zeta)$ , and  $g_2(\zeta)$  are defined by

$$g_0(\zeta) \triangleq \frac{4\zeta^2 + 1}{64\zeta^2}, \quad (15)$$

$$g_1(\zeta) \triangleq \begin{cases} \frac{(4\zeta^2 + 1)^2}{512\zeta^3 \sqrt{\zeta^2 - 1}} \ln \left[ \frac{\zeta^2 - \frac{1}{2} + \zeta \sqrt{\zeta^2 - 1}}{\zeta^2 - \frac{1}{2} - \zeta \sqrt{\zeta^2 - 1}} \right], & \text{for } \zeta > 1 \\ \frac{25}{128}, & \text{for } \zeta = 1 \\ \frac{(4\zeta^2 + 1)^2}{256\zeta^3 \sqrt{1 - \zeta^2}} \left[ \frac{\pi}{2} - \tan^{-1} \left( \frac{\zeta^2 - \frac{1}{2}}{\zeta \sqrt{1 - \zeta^2}} \right) \right], & \text{for } \zeta < 1, \quad \text{and} \end{cases} \quad (16)$$

$$g_2(\zeta) \triangleq \frac{\pi^2 (4\zeta^2 + 1)^3}{1024\zeta^4}, \quad (17)$$

respectively. The damping factor,  $\zeta$ , for a perfect second-order OPFL is given by [19]

$$\zeta \triangleq \frac{1}{2} \sqrt{\frac{\tau_2^2 AK_P}{\tau_1}}. \quad (18)$$

## 111, MEASUREMENT OF LASER FREQUENCY NOISE

As pointed out in the previous section, the performance of the phase tracking loop depends critically on the frequency noise characteristics of the lasers. Therefore accurate knowledge of the laser frequency noise is required in order to design an optimal feedback control. The frequency noise statistics of the Lightwave model 120-01 A lasers were measured by first heterodyne detecting the optical signal and then performing the frequency deviation measurement using an open-loop RF frequency discriminator at the intermediate frequency.

An experimental setup for the IF frequency noise measurement is shown in Fig. 2. The signal from a laser is mixed with an identical local oscillator laser and then detected using a balanced detector. The IF signal is then mixed with an FM-modulated reference signal to provide a calibration for the resulting frequency noise measurements. After the second frequency mixing, the IF signal is subsequently amplified and passed through a bandpass limiter. The passband of the IF is chosen to be sufficiently wide (10 MHz) such that the frequency drift during the measurement period is small compared to the IF bandwidth. The purpose of the bandpass limiter is to provide AM sideband rejection. These AM sidebands, located near 300 kHz, are due to the interaction between signal and LO mean fields with the fluctuations in LO and signal amplitudes. Amplitude-varying noise such as the relaxation oscillation can produce AM sidebands that, if not properly suppressed, can corrupt the frequency noise measurement. Unlike the signal and LO intensity noises that are located near dc and can be suppressed by using the balanced detector configuration, these AM sidebands are located near the IF spectral peak, and cannot be suppressed by using a balanced detector. Since the relaxation oscillation is an amplitude noise and not a frequency noise, inclusion of the AM noise in frequency noise measurements can result in erroneous prediction of the phase tracking loop performance. After bandpass filtering, the

IF is fed into an RF frequency discriminator. The output from the discriminator is then amplified, low-pass filtered, and fed into a dynamic signal analyzer.

The measured frequency noise power spectral density (PSD) of the Lightwave lasers is shown in Fig. 3. The calibration peak at 400 Hz is due to the FM calibration signals. Also shown in the figure is an empirical model of the laser frequency noise consisting a white component, a  $1/f$  component, and a  $1/f^2$  component. The parameters associated with the frequency noise model shown in Fig. 3 are  $k_0 = 0.2$  Hz,  $k_1 = 1.5 \times 10^4$  Hz\*, and  $k_2 = 1 \times 10^7$  Hz<sup>3</sup>. It is seen from Fig. 3 that the power spectral density of the laser frequency fluctuation contains a strong  $1/f^2$  component in addition to the  $1/f$  and white noise components. Furthermore, the measurement confirmed that the white component of the frequency noise is less than 0.2 Hz.

#### IV. DESIGN OF AN OPLL

The total phase error variance can be written, by substituting (5), (9), and (14), into (4), as

$$\sigma_{\phi_e}^2 = MF \left\{ \frac{N_0}{A^2} B_L + k_0 g_0(\zeta) \frac{1}{B_L} + k_1 g_1(\zeta) \frac{1}{B_L^2} + k_2 g_2(\zeta) \frac{1}{B_L^3} \right\}, \quad (19)$$

where  $B_L$ ,  $g_0(\zeta)$ ,  $g_1(\zeta)$ , and  $g_2(\zeta)$  are defined by (6), (15), (16), and (17) respectively. The functions  $g_0(\zeta)$ ,  $g_1(\zeta)$ , and  $g_2(\zeta)$  are plotted in Fig. 4. Note that  $g_0(\zeta)$  is monotonically decreasing as  $\zeta$  increases, and asymptotically approaches 1/16. The minimum of  $g_1(\zeta)$  occurs at  $\zeta = 1.14$  with  $g_1(1.14) = 0.19$ , and  $g_1(\zeta)$  is fairly constant for  $1 < \zeta < 1.5$ . For all practical purposes,  $g_1(\zeta) \approx g_2(1.14) = 0.19$  for  $1 < \zeta < 1.5$ . Unlike the above two cases,  $g_2(\zeta)$  decreases with increasing  $\zeta$ , and reaches a minimum of 1.04 at  $\zeta = 0.71$ , and begins to increase as  $\zeta$  increases further.

The modulation factor  $MF$  in (19) is defined by

$$MF = \left[ 1 - \int_0^\infty |H_1(j2\pi f)|^2 S_a(f) df \right]^{-1}, \quad (20)$$

For binary pulse position modulated (BPPM) signal, the modulation factor can be written approximately as

$$MF = \left[ 1 - \int_0^{\frac{\pi}{2} \frac{B_L}{R_b}} \frac{\sin^4(x)}{x^2} dx \right]^{-1}, \quad (21)$$

where  $R_b$  is the data rate, and it is assumed that  $H_1(j2\pi f)$  is a perfect low pass filter with cut-off frequency  $B_L$ . With this approximation, the modulation factor depends explicitly on the ratio of bandwidth to data rate ( $\frac{B_L}{R_b}$ ). As indicated in (9), the effect of amplitude modulation on the total phase error variance appears as a multiplicative factor. For the case of no modulation or in the limit as  $B_L/R_b$  goes to zero, it can be shown that  $MF = 1$ , and the phase error variance is the bracketed term in the expression (19). Figure 5 shows the  $MF$  as a function of  $B_L/R_b$  for  $0 < B_L/R_b < 2$ . Note that the  $MF$  increases monotonically as  $B_L/R_b$  increases. The implication is that for a fixed data rate, the total phase error variance in (19) increases as loop bandwidth increases in the absence of frequency noise. This agrees with one's intuition that more and more modulation noise passes through the closed loop transfer function,  $H_1(2\pi f)$ , as the loop bandwidth increases, and hence degrades the tracking performance. It can also be seen from Fig. 5, that  $MF$  is roughly equal to 1 for  $B_L/R_b < 0.25$ . This implies that the effect of modulation is negligible for an OPLL with a loop bandwidth smaller than one fourth of the data rate when using amplitude modulation.

Because of the nature of the BPPM input, the OPLL must be able to track a phase step input, during the "off-to-on transition" time of the signal. The height of the phase step input depends on the amount of relative phase drift between the two lasers during the last off period, and the phase error at the "on-to-off transition" instant. A critically damped

( $\zeta = 1$ ) or an overdamped ( $\zeta > 1$ ) loop is desirable in order to minimize the transient effects such as ringing, and overshoots. By emphasizing the requirement of minimizing the transients due to the phase step inputs of the OPLL, an overdamped loop with  $\zeta = 1.5$  was chosen as a practical compromise between the functions  $g_0(\zeta)$ ,  $g_1(\zeta)$ , and  $g_2(\zeta)$ . A loop filter was designed for laboratory demonstrations with  $\tau_2 = 250 \mu\text{sec}$  and  $\tau_1 = 8.8 \text{msec}$ , which results in an overdamped loop ( $\zeta = 1.5$ ) with a loop bandwidth of 10 KHz at baseband signal amplitude of 1 volt.

Using these parameters, the contribution of shot noise, white frequency noise,  $1/f$  frequency noise,  $1/f^2$  frequency noise to total phase error variance can be calculated. Figure 6 shows the contributions to the total phase error variance from each of the noise components, as well as the total phase error variance. The figure was plotted with loop bandwidth from 0 to 20 KHz, and for  $A^2/N_0 = 70 \text{ dB-Hz}$  with no modulation. It can be seen from Fig. 6 that performance of the OPLL is frequency noise limited if the loop bandwidth is less than 3 KHz, and is shot noise limited if the loop bandwidth is greater than 3 KHz. A family of curves representing total phase error variance with different values of  $A^2/N_0$  is plotted in Fig. 7 as a function of loop bandwidth for the case of no modulation. It can be seen from Fig. 7 that the standard deviation of the phase tracking error is less than  $10^\circ$  for  $A^2/N_0 > 60 \text{ dB-Hz}$  for an OPLL with a loop bandwidth of 10 KHz. This verifies that the linear approximation made throughout the analysis is valid when  $A^2/N_0 > 60 \text{ dB-Hz}$ .

It is seen from Figs. 6 and 7 that the phase error variance decreases with increasing loop bandwidth until a minimum is reached. Further increase in loop bandwidth will result in an increased phase error variance. The existence of an optimal bandwidth or minimum phase error variance is also seen from (19). Assuming that  $\zeta = 1.5$ ,  $MF = 1$ , and the measured frequency noise parameters, the optimal loop bandwidth can be plotted

as a function of the carrier signal-to-noise ratio (CNR). Figure 8 shows that the optimal loop bandwidth increases as  $A^2/N_0$  increases. The performance of the OPLL becomes frequency noise limited as the CNR increases, and therefore better tracking performance can be obtained by widening the loop bandwidth. Although Figs. 6-8 are plotted for the case of no modulation (it is important to note here that they are equally valid for the case of tracking amplitude modulated signals as long as  $B_L/R_b < 0.25$ ).

## V. OPLL EXPERIMENT

A simplified block diagram of an OPLL experiment is shown in Fig. 9. The received optical signal is detected using a balanced detector configuration. The balanced detector configuration is used to cancel the LO laser intensity noise [21]. The IF signal is filtered through an IF bandpass filter and further mixed down to baseband using a RF mixer and a stable frequency reference. The error signal at the output of the mixer is filtered by a loop filter to obtain an estimate of the phase error between the received and the LO laser signals. The output signal of the loop filter is then fed back into the frequency tuning input of the LO laser.

Frequency tuning of Lightwave model 120-01 A lasers is achieved through its two BNC inputs. By applying a voltage to the thermal BNC input, continuous frequency tuning is possible over a range of 16 GHz [22]. However thermal tuning is generally slow to stabilize at each new frequency, and much faster tuning is required for phase locked operation. A small PZT stack deposited on top of the Nd:YAG crystal reacts to the control input voltage by applying stress to the lasing cavity. This alters the physical characteristics of the lasing cavity slightly, and hence the lasing frequency of the laser with a guaranteed range of 30 MHz and a response time of a few microseconds [22, 23]. Tuning constant  $K_P$  of approximately 1.2 MHz/V has been measured for the 1.0 laser.

Although the PZT controller is sufficiently fast to track the instantaneous phase of the loop, it does not possess the wide frequency tuning range needed to compensate for the large drift in lasing frequency. Ambient temperature drifts can cause the lasing frequency to drift by as much as  $1.7 \text{ GHz}/^\circ\text{C}$ . Consequently, a frequency compensation loop must be included to maintain the PZT controlled loop at the center of its dynamic range. Temperature control is accomplished by applying a proper compensating signal at the thermal control input. This compensating signal is obtained by scaling and integrating the loop filter output appropriately.

A phase tracking experiment was performed, and the measured phase error variance vs. loop bandwidth is plotted in Fig. 10. Also shown in the figure are the theoretical predictions derived using a white frequency noise of 6 KHz linewidth [12], and results derived using the frequency noise model given in Fig. 3. It is seen from Fig. 10 that the predicted phase error variance using a white frequency noise of 6 KHz linewidth is 3-4 orders of magnitude larger than experimentally measured values. However, measured phase error variance closely matches the theoretical predictions using OPLL theory derived from the noise model given in section II.

## VI. CONCLUSIONS

Theoretical analysis indicated that the phase error variance of an OPLL, can be written as a combination of the contribution from shot noise, modulation noise, and frequency noise. The frequency noise contribution can be evaluated by modelling the frequency noise spectrum as a sum of a white component, a  $1/f$  component, and a strong  $1/f^2$  component. Contributions of shot noise and of each frequency noise component to total phase error variance of the OPLL have been derived in closed form to display their explicit relationships to loop bandwidth and damping factor. The effect of amplitude modulation on total phase

error variance of the  $\sigma^2$ , appears as a multiplicative factor, and is negligible for loop bandwidths smaller than one fourth of the data rate.

The design choice of the loop filter can be made by considering the frequency noise components, and the transient effects due to phase step inputs occurring from the nature of amplitude modulated signal. It can be concluded that if moderate effort in characterizing the frequency noise is spent initially, then the system performance can be predicted accurately. Furthermore, an OPLL can be designed successfully to operate under weak incident signal power with optimum tracking bandwidth.

#### ACKNOWLEDGMENTS

The authors would like to thank Mr. James R. Lesh, Dr. Sami M. Hinedi, Dr. Marvin K. Simon, and Randy Bartman of Jet Propulsion Laboratory, and Professor William C. Lindsey of University of Southern California for their helpful discussions. The research described in this paper was carried out by the Jet Propulsion Laboratory, California Institute of Technology, under contract with the National Aeronautics and Space Administration.

#### REFERENCES

- [1] R. M. Gagliardi, and S. Karp, *Optical Communications*, John Wiley & Sons, 1976.
- [2] C. N. Georghiades, and D. L. Snyder, "Receiver Performance for Heterodyne Optical Communications," *IEEE Trans. Commun.*, vol. COM-34, no. 11, Nov., 1986, pp. 1096-1104.
- [3] W. C. Lindsey, and Simon, *Telecommunications Systems Engineering*, Englewood Cliffs, NJ: Prentice-Hall, Inc., 1973.
- [4] I. G. Kazovsky, "Decision-Driven Phase-Locked Loop for Optical Homodyne Re-

- ceivers: Performance Analysis and Laser Linewidth Requirements" *IEEE J. Lightwave Technol.*, vol. LT-3, no. 6, Dec., 1985, pp. 1238-1247.
- [5] C. N. Georghiades, and D. L. Snyder, "A Proposed Receiver Structure for Optical Communication Systems that Employ Heterodyne Detection and a Semiconductor Laser as a Local oscillator," *IEEE Trans. Commun.*, vol. COM-33, no. 4, Apr., 1985, pp. 382-384.
- [6] I. G. Kazovsky, "Balanced Phase-Locked Loop for Optical Homodyne Receivers: Performance Analysis, Design Considerations and Laser Linewidth Requirements" *IEEE J. Lightwave Technol.*, vol. LT-4, no. 2, Feb., 1986, pp. 182-195.
- [7] I. G. Kazovsky, "Performance Analysis and Laser Linewidth Requirements for Optical PSK Heterodyne Communications Systems" *IEEE J. Lightwave Technol.*, vol. LT-4, no. 4, Apr., 1986, pp. 415-425.
- [8] V. W. S. Chan, L. L. Jeromin, and J. F. Kaufmann, "Heterodyne Lasercom Systems using GaAs lasers for ISI applications," in *Proc. Int. Conf. Commun.*, Boston, MA, June, 1983, pp. 1201-1207.
- [9] T. Y. Fan and R. L. Byer, "Diode laser-pumped solid-state lasers," *IEEE J. Quantum Electron.*, vol. QE-24, no. 6, June, 1988, pp. 895-912.
- [10] R. L. Byer, "Hertz linewidth diode pumped solid state lasers," *IEEE LEOS Annual Meeting*, Orlando FL, Oct. 17-20, 1989.
- [11] T. J. Kane, A. C. Nilsson, and R. L. Byer, "Frequency Stability and offset locking of a laser-locked Nd:YAG monolithic nonplanar ring oscillator," *Opt. Lett.*, vol. 12, no. 3, March, 1987, pp. 175-177.

- [12] S. P. Bush, A. Gungor, and C. C. Davis, "Studies of the coherent properties of a diode-pumped Nd:YAG ring laser," *Appl. Phys. Lett.*, vol. 53, no. 8, Aug., 1988, pp. 646-647.
- [13] P. Fritschel, A. J. Jeffries, and T. Kane, "Frequency fluctuation of a diode-pumped Nd:YAG ring laser," *Opt. Lett.* vol. 14, no. 18, Sept. 1989, pp. 993-995.
- [14] L. G. Kazovsky and D. A. Atlas, "Miniature Nd:YAG lasers: noise and modulation characteristics" *IEEE J. Lightwave Technol.*, vol. 17-8, no. 3, March, 1990, pp. 294-301.
- [15] K. J. Williams, L. Goldberg, R. D. Esman, M. Dagenais, and J. F. Weller, "6-34 GHz off-set phase-locking of Nd:YAG 131911111 nonplanar ring lasers," *Electron. Lett.*, vol. 25, no. 8, Aug. 1989.
- [16] C.-C. Chen, M. Z. Win, *et. al.*, "Coherent link demonstration for space communications," OSA Annual Meeting, Orlando, FL, October 1989.
- [17] T. Day, A. Farinas, and R. Byer, "Demonstration of a low bandwidth 1.06  $\mu\text{m}$  optical phase locked loop for coherent homodyne communication," *IEEE Photon Technol. Lett.*, vol. 2, no. 4, Apr., 1990, pp. 294-296.
- [18] A. J. Viterbi, *Principles of Coherent Communications*, New York :McGraw-Hill, Inc., 1962.
- [19] W. C. Lindsey, *Synchronization Systems in Communication and Control*, Englewood Cliffs, NJ: Prentice-Hall, Inc., 1972.
- [20] I. S. Gradshteyn and I. M. Ryzhik, *Tables of Integrals, Series, and Products, Corrected and Enlarged Edition*, Orlando, Fl., Academic Press, Inc., 1980, pp. 67, section 2.161

- [21] G. L. Abbas, V. W. S. Chan, and J. H. Yee, "A Dual-Detector optical Heterodyne Receiver for Local Oscillator Noise Suppression," *J. Lightwave Technol.*, vol. LT-3 no. 5, Oct. 1985, pp. 1110-1122,
- [22] Specification Sheet, *Diode Pumped Solid State Ring Laser, Series 120*, Lightwave<sup>TM</sup> Electronics Inc.
- [23] T. J. Kane, E. A. P. Cheng, "Fast frequency tuning and phase locking of diode-pumped Nd:YAG ring laser," *Opt. Lett.*, vol. 13, no. 11, Nov., 1988, pp. 970-972.

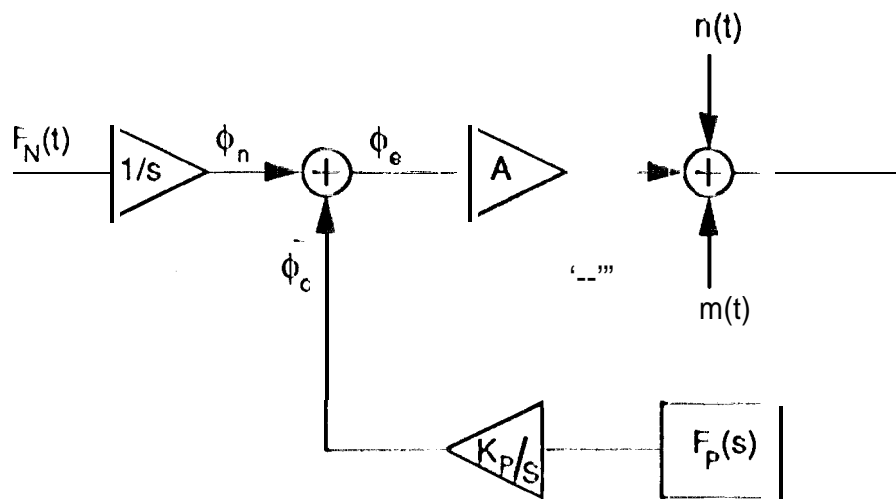


Figure 1, Block diagram of the linearized OPLL.

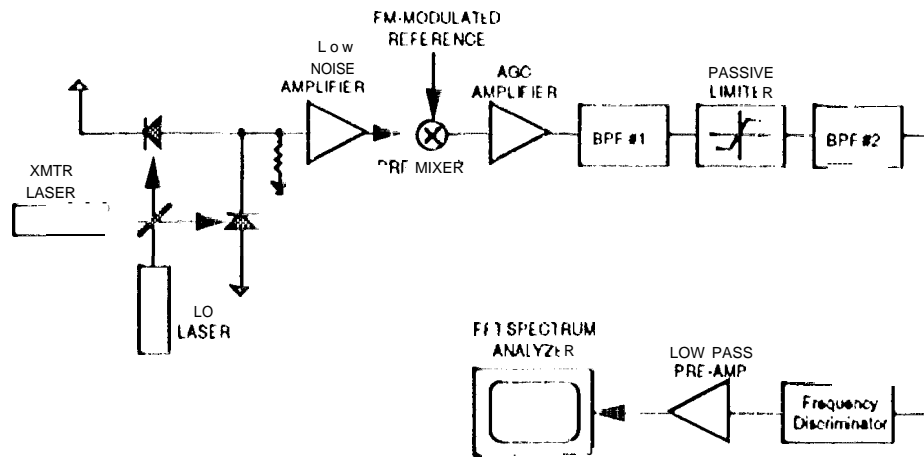


Figure 2. Configuration of the IF frequency noise measurement experiment.

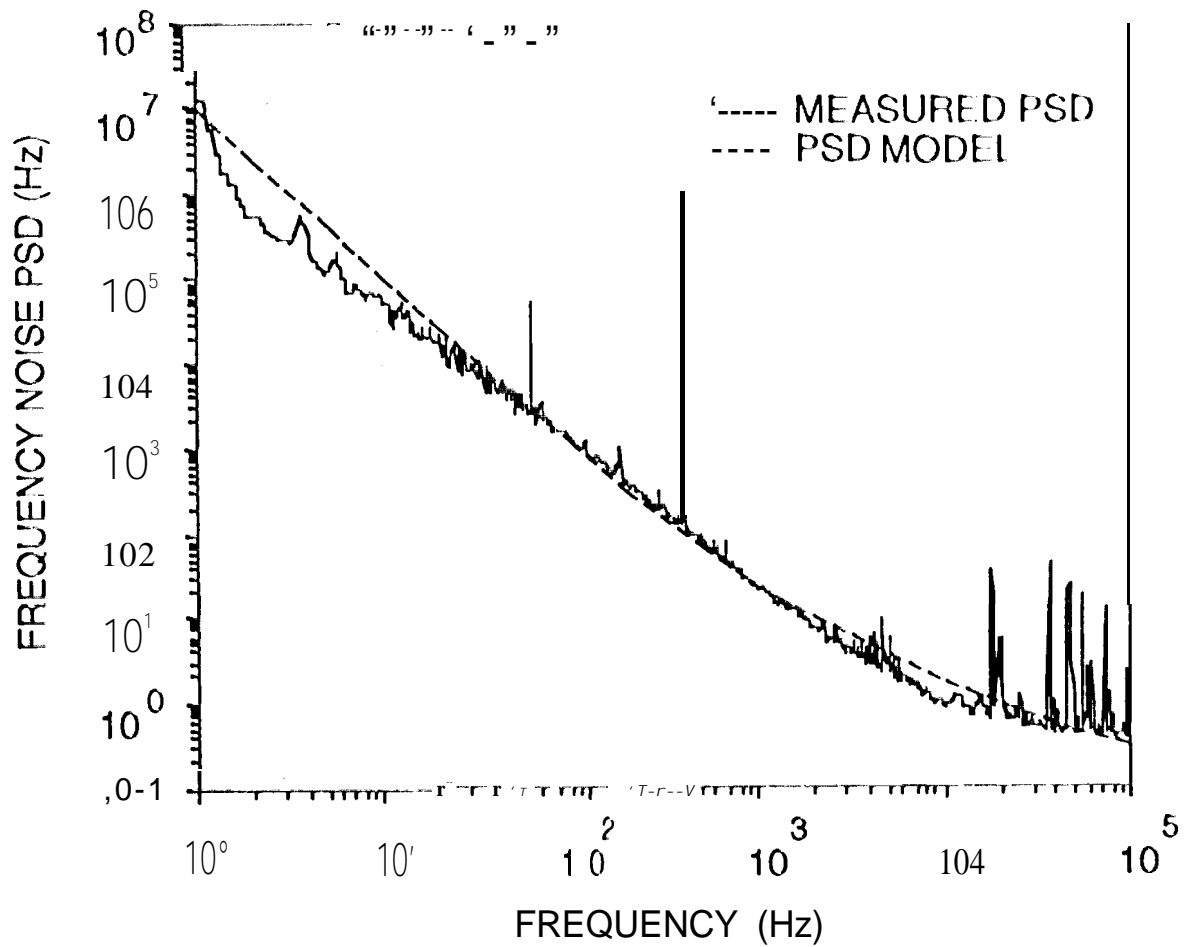


Figure 3. Measured frequency noise floor of the Lightwave nonplanar ring oscillator lasers and the theoretical model used to derive the phase tracking loop performance.

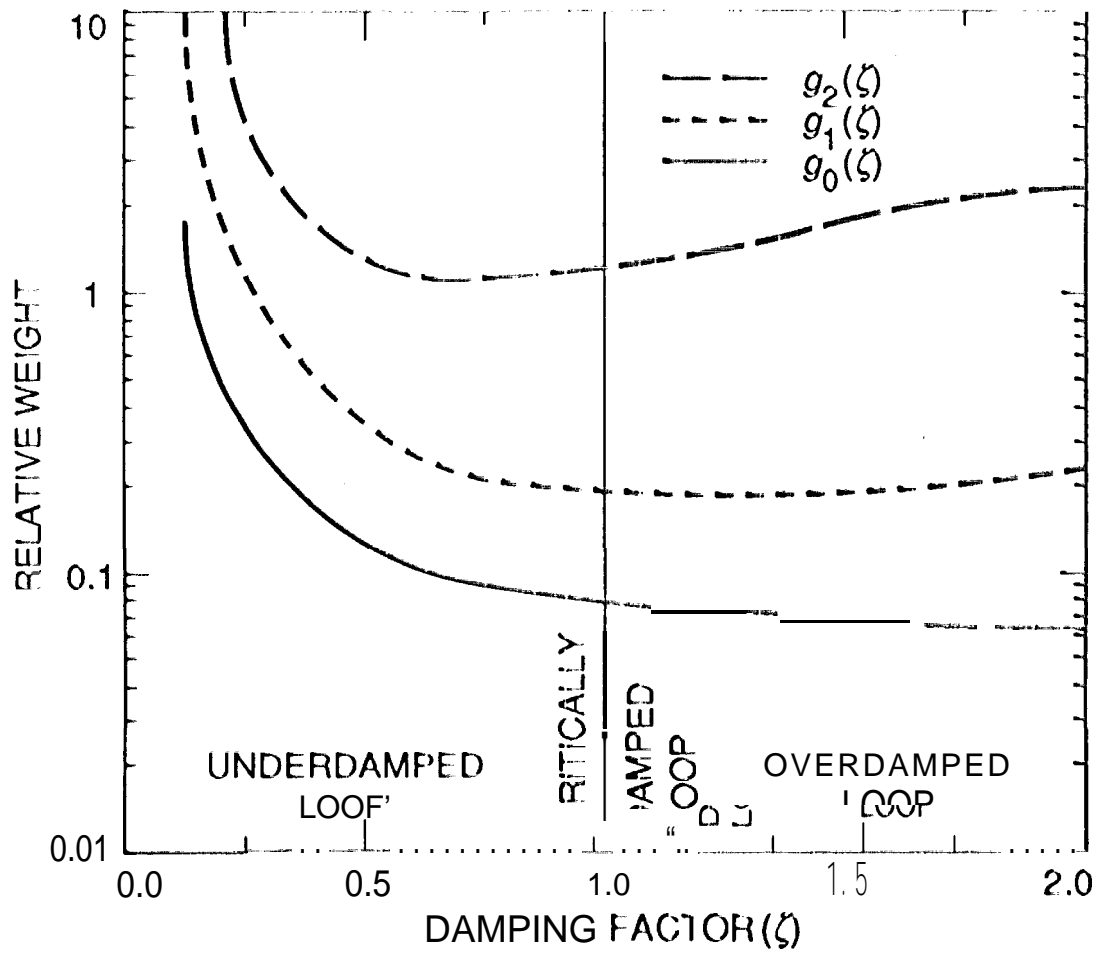


Figure 4. Relative weight of  $g_0(\zeta), g_1(\zeta), g_2(\zeta)$  as a function of  $\zeta$ .

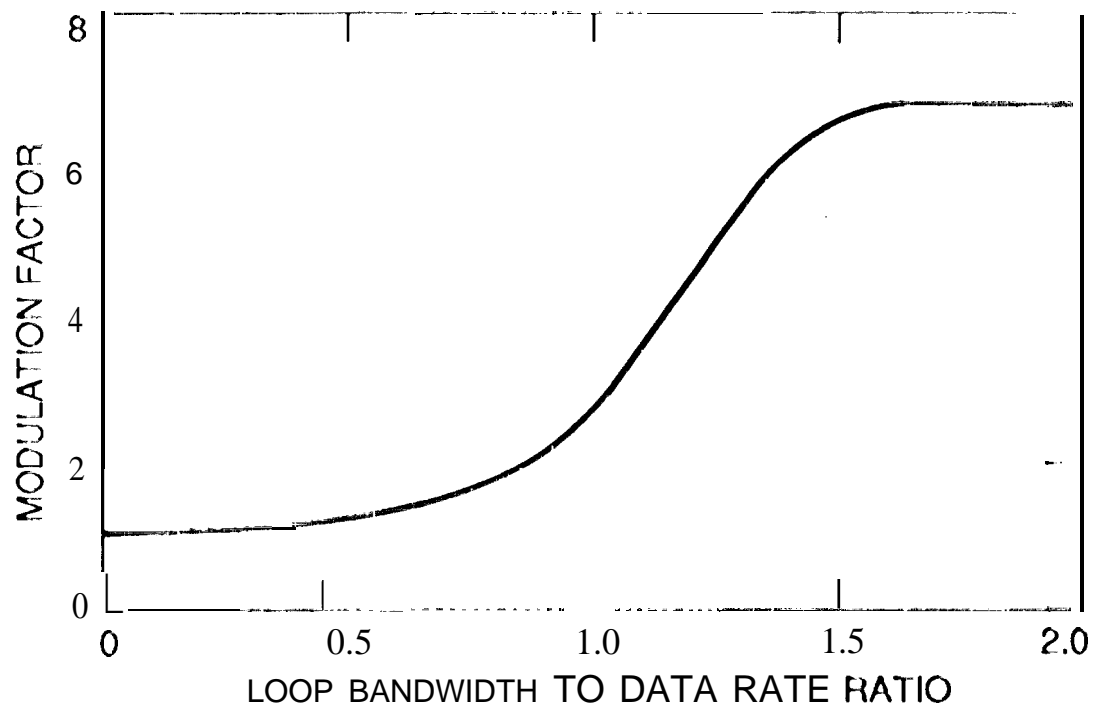


Figure 5. Modulation factor as a function of loop bandwidth to data rate ratio,  $B_L/R_b$ , for  $0 < B_L/R_b < 2$ .

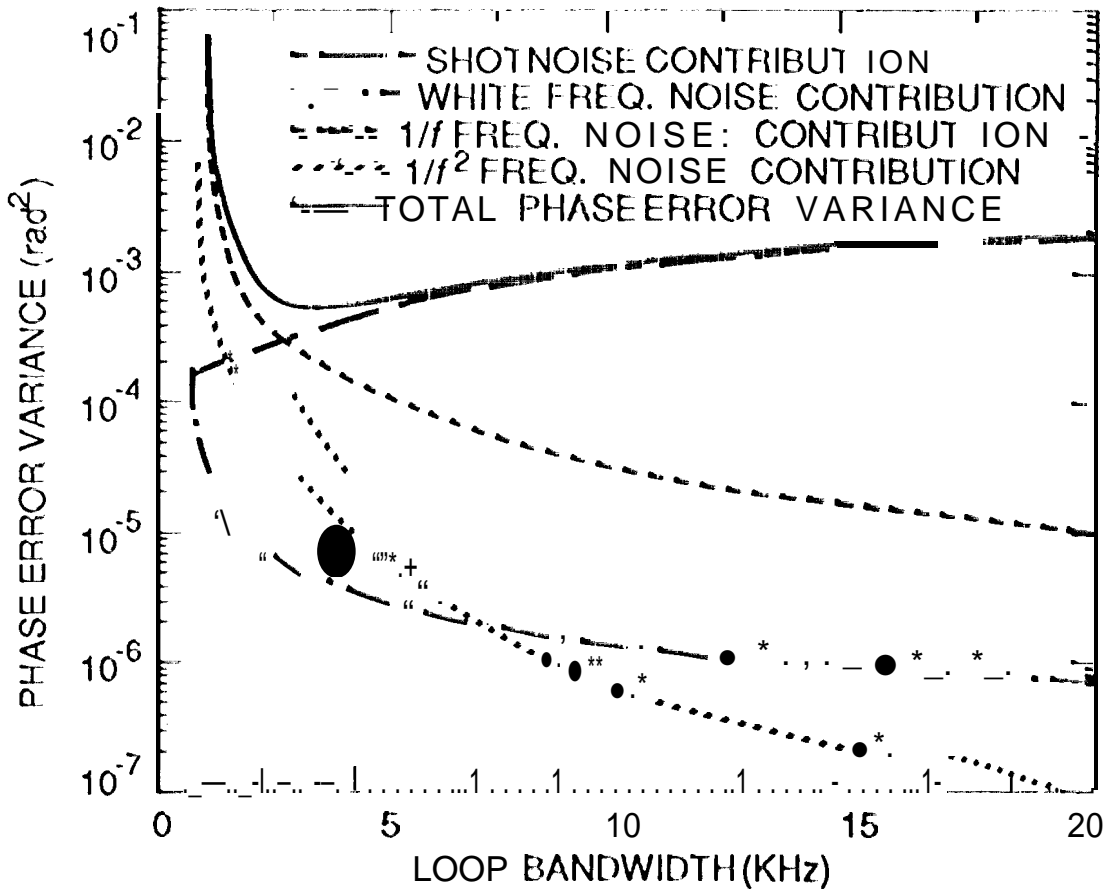


Figure 8 Contributions of each noise components to total phase error variance as a function of loop bandwidth for  $A^2/N_n = 70$  dB-Hz,  $k_0 = 0.2$  Hz,  $k_1 = 1.5 \times 10^4$  Hz<sup>2</sup>,  $k_2 = 1 \times 10^7$  Hz<sup>3</sup>, and  $MF = 1$ .

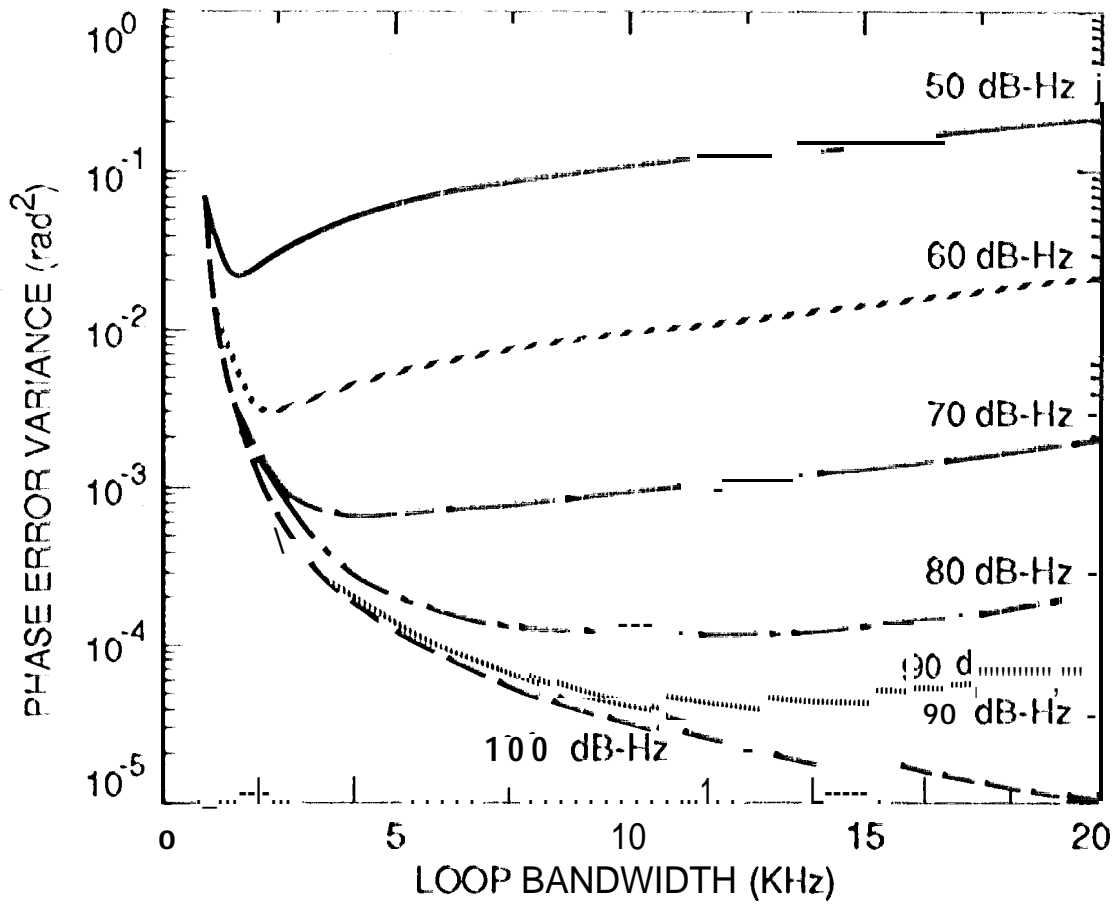


Figure 7. Total phase error variance as a function of loop bandwidth for  $k_0 = 0.2 \text{ Hz}$ ,  $k_1 = 1.5 \times 10^4 \text{ Hz}^2$ ,  $k_2 = 1 \times 10^7 \text{ Hz}^3$ , and  $MF = 1$ .

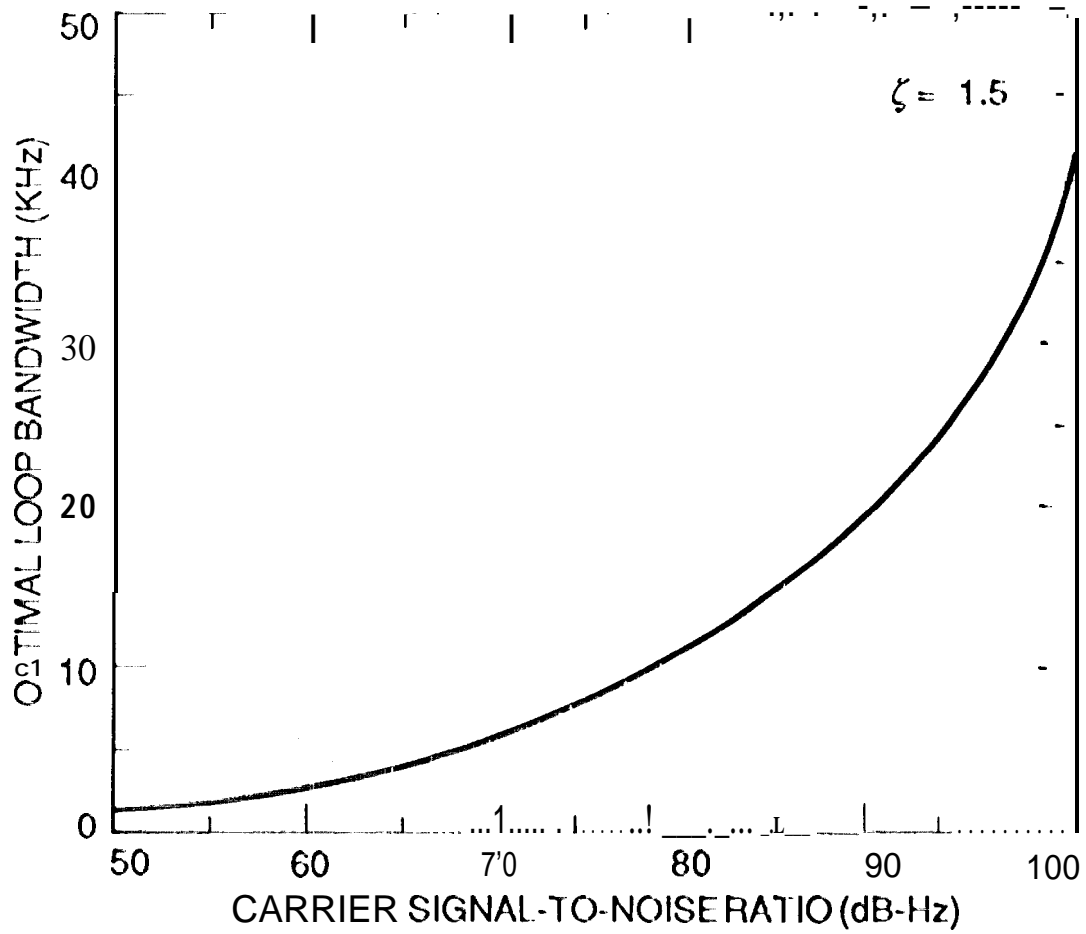


Figure 8. Optimal loop bandwidth as a function of  $A^2/N_0$ , for  $\zeta = 1.5$ ,  
 $k_0 = 0.2$  Hz,  $k_1 = 1.5 \times 10^4$  Hz<sup>2</sup>,  $k_2 = 1 \times 10^7$  Hz<sup>3</sup>, and  $MF = 1$ .

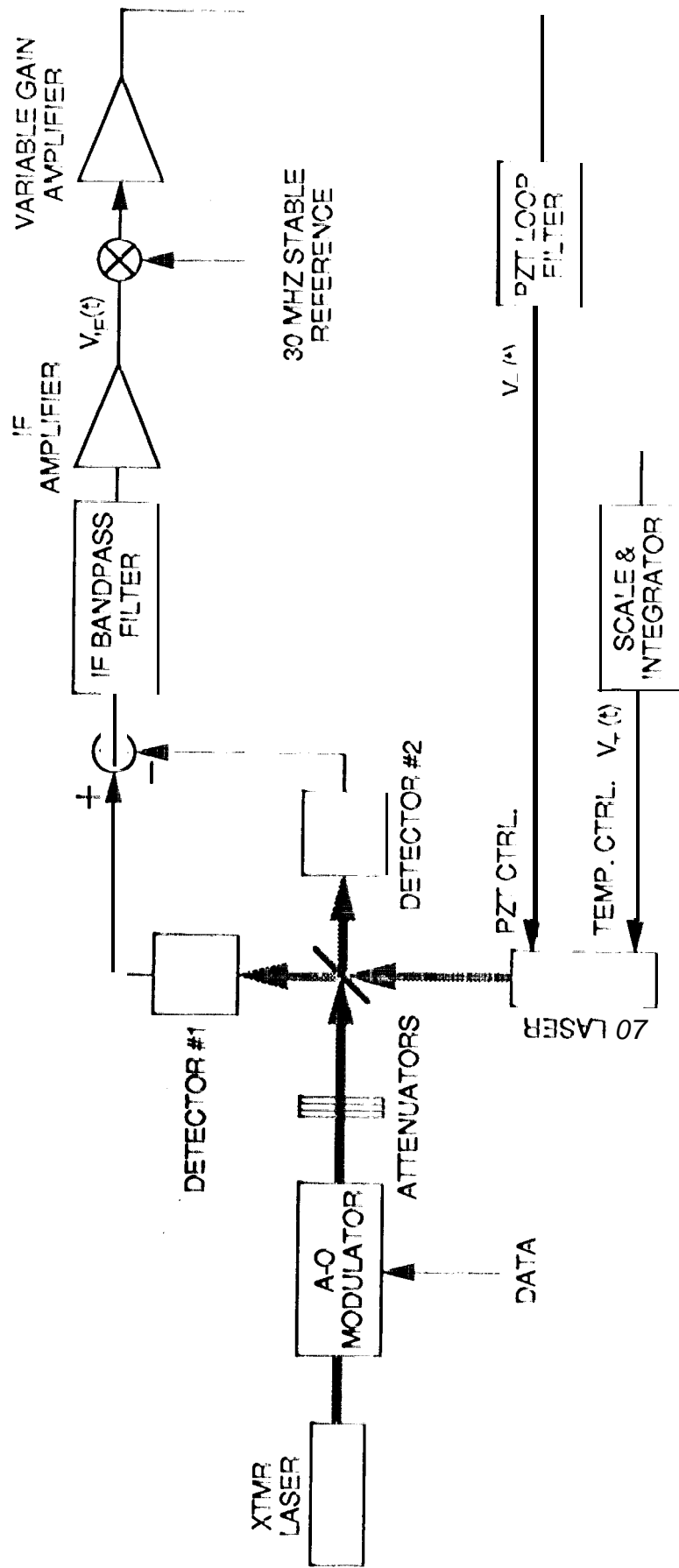


Figure 9. Simplified block diagram of the optical phase-locked loop (OPLL) experiment.

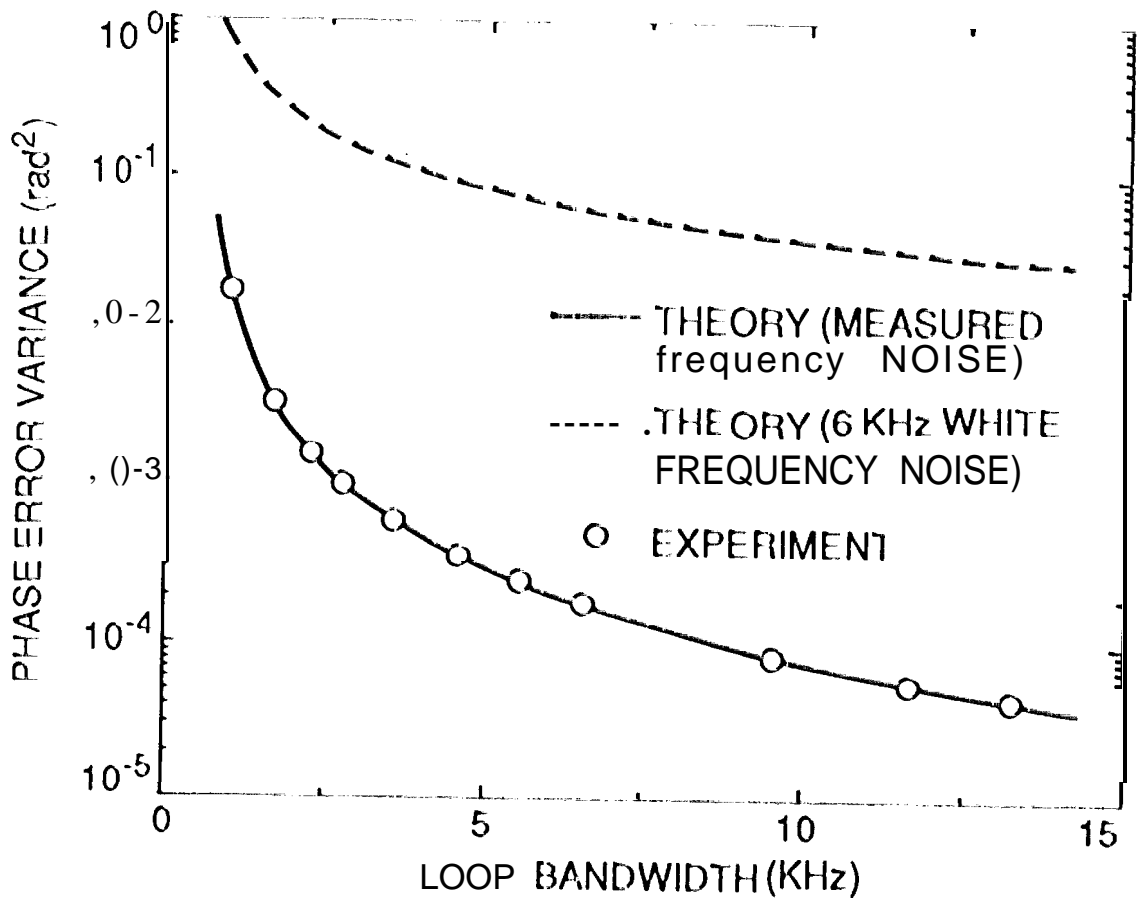


Figure 10. Measured phase error variance from the phase tracking loop experiment. Also shown is the theoretically predicted phase error variance derived from the frequency noise model given in section III, as well as the 6 KHz white frequency noise model.